




# Investigations on structural and magnetic properties of M-type hexagonal ferrite $\text{Ba}_{0.5}\text{Sr}_{0.5}\text{Co}_x\text{La}_x\text{Fe}_{12-2x}\text{O}_{19}$ in X-band

Shally Gujral<sup>1</sup>, Kamaljit Singh Bhatia<sup>2</sup>, Harjitpal Singh<sup>3</sup>, Harsimrat Kaur<sup>3,\*</sup> , and Nancy Gupta<sup>4</sup>

<sup>1</sup>Department of Research and Development, Research Scholar IKGPTU, Jalandhar, India

<sup>2</sup>Department of ECE, G.B. Pant Institute of Engineering & Technology, Pauri Garhwal 246194, Uttarakhand, India

<sup>3</sup>Department of ECE, CTIEMT Shahpur Jalandhar, Punjab, India

<sup>4</sup>Department of ECE, Lyallpur Khalsa College of Engineering, Jalandhar, India

Received: 25 June 2020

Accepted: 8 December 2020

Published online:

3 January 2021

© The Author(s), under exclusive licence to Springer Science+Business Media, LLC part of Springer Nature 2021

## ABSTRACT

The typical ceramic method was used to synthesize the composition of M-type hexagonal ferrite  $\text{Ba}_{0.5}\text{Sr}_{0.5}\text{Co}_x\text{La}_x\text{Fe}_{12-2x}\text{O}_{19}$  by substituting  $\text{Co}^{2+}$  and  $\text{La}^{3+}$ -doping ions ( $0.0 \leq x \leq 1.0$  with steps of  $x = 0.2$ ). The phase-related information of composition was examined by X-ray diffraction (XRD). The microwave absorption of composed material was examined related to doping, thickness, and frequency from (8.2–12.4) GHz by using standard testing instrument. Mechanisms of impedance matching along with quarter wavelength matching have been used for calculation of microwave absorption of composed material. Enhanced microwave absorption of 97% was obtained with  $x = 0.2$  at frequency of 10.75 GHz and thickness 1.9 mm. Also, absorption bandwidth of 0.07 GHz ( $-10 \text{ dB} \leq \text{RL} \leq -20 \text{ dB}$ ) and 0.2 GHz ( $\text{RL} \geq -20 \text{ dB}$ ) was observed.

## 1 Introduction

Today, due to the enormous growth of wireless technology, concerned high-speed devices working at microwave frequency region have created electromagnetic pollution which further caused electromagnetic interference (EMI). It renders the faulty operation of electronic devices. The high-speed devices working at GHz frequency range generate harmonics which increases bit error rate (BER) in the received content by the receiver side. Moreover, if the

width of printed circuit board (PCB) copper paths is approximately equal to a quarter wavelength ( $\lambda/4$ ) of the applied high-frequency signal, then these paths act like an antenna which generates false radiation mentioned as EMI. There are some microwave absorbing materials that can be used to control/attenuate EMI radiation from RADAR, military, satellite, and other high-frequency wireless devices [1–4].

Due to the best magnetic properties, ferrites can provide better results in microwave absorption as compared to standard dielectric substrates. M-type

Address correspondence to E-mail: er.harsimrat@gmail.com

hexagonal ferrites are ferromagnetic materials whose electrical and magnetic properties can be varied with doping of external materials which offer required resistance to EMI interference at the high-frequency range. They drop the undesirable eddy currents with their extreme resistivity in the microwave frequency range [5–8]. Many researchers have informed the microwave absorption features in various materials. Mortazavinik and yousefi [9] suggested synthesizing of strontium hexaferrite with doping of  $\text{Co}^{2+}$ ,  $\text{Zr}^{4+}$ , and  $\text{Zr}^{2+}$  and obtained  $-20$  dB reflection loss with 90% EMI absorption. Singh et al. [10] examined properties of barium hexaferrite and analyzed the static and dynamic properties of the same. Singh et al. [11] prepared M-type barium strontium hexaferrite with substitution of  $\text{Co}^{2+}$  and  $\text{Sn}^{4+}$  ions and found an increase in magnetic loss, thus suitable for microwave absorption. Further, Bhatia et al. [12] proposed that microwave absorption got improved by adding indium in Ba-Sr M-type hexagonal ferrite. The dielectric properties were found superior to magnetic properties in X-band. Also, Hou et al. [13] anticipated spinel ferrite with one layer and two-layer of nickel and zinc combination and then represented the maximum reflection loss with double layer hexaferrite. Zhang et al. [14] presented  $\text{Co}_{1-x}\text{S}$  microspheres, which obtained reflection loss  $-46.1$  dB. Tran et al. [15] discussed that M-type hexagonal ferrite  $\text{BaFe}_{12}\text{O}_{19}$  with doping of strontium changed the magnetic properties of the structure. Li et al. [16] proposed carbon-dependent nanocomposite and reported reflection loss of  $-55.8$  dB and got maximum microwave absorption. Septiani [17] suggested M-type strontium hexagonal ferrite with doping of Co and Ti and observed a decrease in coercivity and reflection loss of  $-31$  dB. Yan et al. [18] suggested nanocomposite with polyaniline-filled structure got different values of permittivity and permeability to achieve maximum EMI reduction. Trudel et al. [19] synthesized barium hexagonal ferrite with substitution of Al and Cr ions and then observed a high value of coercivity. Peymanfar et al. [20] suggested the preparation of  $\text{CuCr}_2\text{O}_4$  sample using a sol-gel technique and obtained reflection loss of  $-65.57$  dB and absorption bandwidth of 7.73 GHz. Jiao et al. [21] synthesized  $\text{Fe}_3\text{O}_4$  and graphene oxide showed a reflection loss of  $-47.2$  dB. Kaur et al. [22] examined M-type hexagonal ferrite  $\text{Ba}_{0.5}\text{Sr}_{0.5}\text{Co}_x\text{In}_x\text{Fe}_{12-2x}\text{O}_{19}$  and obtained reflection loss of  $-39.99$  dB. Trukhanov et al. [23] examined  $\text{Ba}(\text{Fe}_{1-x}\text{Sc}_x)_{12}\text{O}_{19}$  and found

deep relation of  $\text{Sc}^{3+}$  ions with diamagnetic ions. The author investigated microwave properties in (20–60) GHz frequency region and concluded that it can be used as microwave absorber for high-frequency applications. Afshar et al. [24] prepared  $\text{SrFe}_{12}\text{O}_{19}$  and observed  $-14.5$  dB reflection loss. Dhruv et al. [25] suggested  $\text{Sr}_3\text{Co}_{2-x}\text{Ga}_x\text{Fe}_{24}\text{O}_{41}$  with substitution of Gallium showed permittivity value (8–14) and permeability value (1–1.4) in X-band. Kaur et al. [26] proposed M-type strontium hexaferrite with substituting lanthanum and observed properties in K-band found best RL of  $-30$  dB and absorption bandwidths of 2 GHz for composition  $x = 0.25$ . Later, absorption bandwidths were increased in Ka band to (3.43, 2.62, 3.93, and 2.3) GHz. Then, Jafarian et al. [27] used structures of core-shell with metal particle of Cu along with Ppy hexaferrite and observed with  $-22$  dB value of return loss at a frequency of 10.8 GHz and pallet thickness of 2 mm. Also, Garg et al. [28] synthesized strontium hexaferrite with titanium silicon carbide and obtained RL of  $-39.67$  dB at frequency of 9.46 GHz with sample thickness of 2 mm. Also, the bandwidth of 2.77 GHz was investigated.

In the present research, hexagonal ferrite (M-type) with composition  $\text{Ba}_{0.5}\text{Sr}_{0.5}\text{Co}_x\text{La}_x\text{Fe}_{12-2x}\text{O}_{19}$  is prepared using a standard ceramic technique at temperature of 1100 °C with composition ( $0.0 \leq x \leq 1.0$  with steps of  $x = 0.2$ ) and microwave absorption is investigated using mechanisms of quarter wavelength and impedance matching. In the recent research article [29], we already examined the same series at 1150 °C and the results get published in a reputed journal.

## 2 Experimental work

In this experiment, the standard ceramic technique was used to synthesize  $\text{Ba}_{0.5}\text{Sr}_{0.5}\text{Co}_x\text{La}_x\text{Fe}_{12-2x}\text{O}_{19}$ , hexagonal ferrite (M-type) with composition ( $0.0 \leq x \leq 1.0$  with steps of  $x = 0.2$ ). For this, the raw material was taken, weighted using a weighing machine, and mixed in agate and pestle mortar with distilled water for 8 h as per chemical equation; then, grinding was done by using an attached grinder to get a homogeneous mixture. This mixture was placed in alumina crucibles, which were kept in the electric furnace, with starting temperature set at 0 °C. Then that mixture was pre-sintered for 10 h at 1000 °C.

Thus, calcined powder was obtained and was crushed again manually and grounded in agate and pestle mortar for 8 h with distilled water. Polyvinyl alcohol was used to bind granules and sieving was done using the sieve of size 220 B.S.S to separate different sizes of granules. Rectangular-shaped pallet was prepared from different sizes of granules with a hydraulic press by applying the pressure of 75 KN per square meter. The concluding sintering was performed for 15 h at 1100 °C.

### 3 Results with discussion

#### 3.1 X-ray diffraction (XRD) analysis

XRD analysis was used to find structural information of crystalline structure and phase purity of synthesized material. X-ray diffraction (XRD) analysis was executed (with Philips X'pert diffractometer) to examine the phase purity of prepared powder. XRD graphs of hexagonal ferrite (M-type)  $\text{Ba}_{0.5}\text{Sr}_{0.5}\text{Co}_x\text{La}_x\text{Fe}_{12-2x}\text{O}_{19}$  with  $(0.0 \leq x \leq 1.0)$  with steps of  $x = 0.2$  are represented in Fig. 1. Hexagonal (M-type) crystalline structure parameters are well matched with JCPDS file no. 51-1879,  $a = 5.8862$  (Å),  $c = 23.137$  (Å),  $V = 694.24$  (Å<sup>3</sup>) and space group of  $P6_3/mmc$  in XRD patterns. Some traces of hematite ( $\alpha\text{-Fe}_2\text{O}_3$ ) phase have also been seen as a minor phase in the substituted ( $x > 0.2$ ) compositions (JCPDS file no. 88-2359,  $a = b = 5.112$  Å,  $c = 13.82$  Å).

Lattice parameters [ $a = b$  and  $c$ ] were formulated by equation given below:

$$\frac{1}{d_{hkl}^2} = \frac{4}{3} \left( \frac{h^2}{a^2} + \frac{hk}{a^2} + \frac{k^2}{a^2} \right) + \frac{l^2}{c^2} \quad (1)$$

where ( $a = b \neq c$ ) along with ( $\alpha = \beta = 90^\circ$ ) with ( $\gamma = 120^\circ$ ) for hexagonal structural structure,  $d_{hkl}$  as lines of d-spacing in XRD graph with  $h, k,$  and  $l$  as Miller indices.

The variation of lattice constant ' $a$ ' is small in comparison with ' $c$ ' by addition of doping materials  $\text{Co}^{2+}$  and  $\text{La}^{3+}$  that is the standard feature of hexagonal ferrite. The differences in radii of ionic dopants  $\text{Fe}^{3+}$  (0.64 Å),  $\text{La}^{3+}$  ions (1.15 Å) and  $\text{Co}^{2+}$  (0.72 Å) caused variation in the lattice parameters with doping.

The mixing of doping ions  $\text{Co}^{2+}$  and  $\text{La}^{3+}$  in the lattice structure of hexagonal ferrite (M-type) is indicated by increase in parameters of lattice and unit

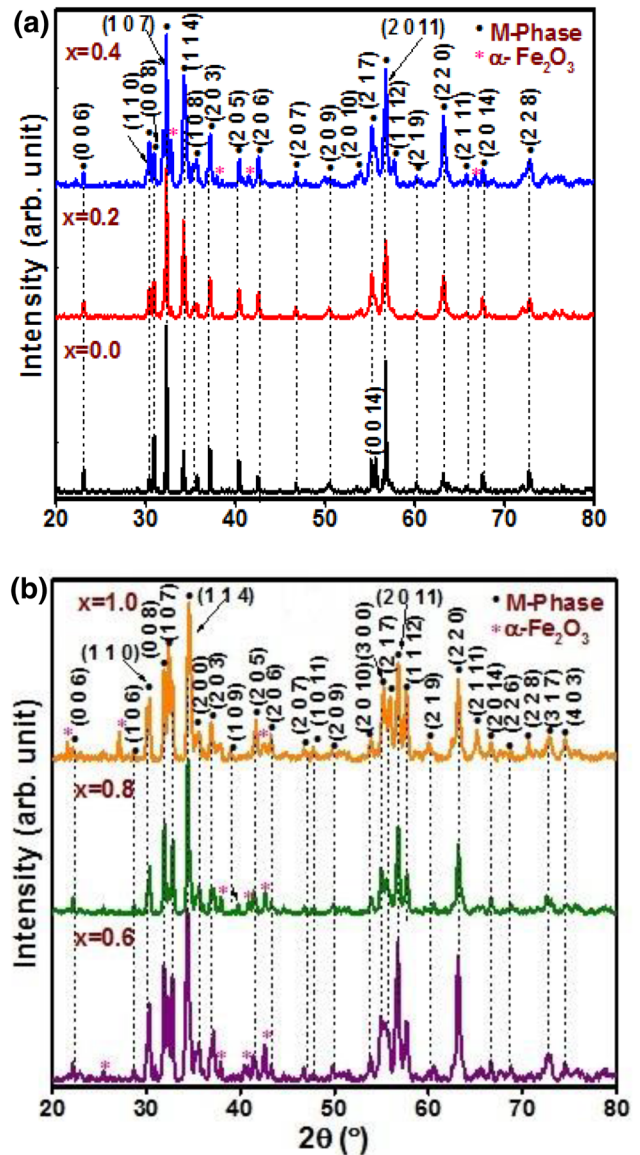


**Fig. 1** a and b XRD analysis of ferrite  $\text{Ba}_{0.5}\text{Sr}_{0.5}\text{Co}_x\text{La}_x\text{Fe}_{12-2x}\text{O}_{19}$  with compositions  $(0.0 \leq x \leq 1.0)$  with steps of  $x = 0.2$

cell volume, which is persistent throughout the literature. The lattice parameter ratio ' $c/a$ ' ratio (3.929–3.936) existed in the required range also displayed structure of hexagonal ferrite (M-type). Structure type can be represented by  $c/a$  ratio: If the  $c/a < 3.98$ , the structure formation is considered as M-type. The bulk density values exist in (3.62–4.37)  $\text{g}/\text{cm}^3$  and the range of X-ray density is (5.20–5.31)  $\text{g}/\text{cm}^3$ . Also, X-ray density is found higher that suggested the presence of pores developed due to higher atomic mass of the doped compositions ( $\text{Co}$ -58.93amu,  $\text{Fe}$ -55.84amu,  $\text{La}$ -138.90amu) in

comparison with un-doped composition because there is a direct relationship between atomic weight and X-ray density. There is an inverse relationship between X-ray density and unit cell volume; thus, if density of X-ray increases, unit cell volume decreases and vice versa (as in Table 1).

### 3.2 Hysteresis properties (frequency-dependent)

Figure 2 represents hysteresis loops with compositions ( $0.0 \leq x \leq 1.0$  with steps of  $x = 0.2$ ) for Ba-Sr hexagonal ferrite. Hysteresis loops were recorded at room temperature with a vibrating sample magnetometer (i.e., SQUID, quantum design) under 10kOe applied field. Low coercivity is the main requirement for designing a microwave absorber. The law of saturation is used to examine the anisotropy field ( $H_a$ ) as well as saturation magnetization ( $M_s$ ). The substitution results in nonlinear reduction in  $H_c$ . The value of  $H_c$  is related to the extrinsic and intrinsic effect. The extrinsic factor ( $H_e$ ) is in direct relation with porosity whereas it is inversely proportional to grain size. The intrinsic factor depends on the anisotropy field ( $H_a$ ). With the doping of  $\text{Co}^{2+}$  and  $\text{La}^{3+}$ , there is nonsystematic variation of  $H_a$  and  $H_c$ . The value of  $H_a$  increases with low porosity as shown in Table 1. The lowest  $H_a$  is 6.15 kOe for  $x = 0.8$  and the highest value is 10.45 kOe for  $x = 0.4$ . The small porosity in  $x = 0.4$  increases the  $H_a$  value. The site occupancy of 4f2 and 2b sites by  $\text{Co}^{2+}$  and  $\text{La}^{3+}$  dopants also influences the value of  $H_a$ . There is nonlinear increase in saturation magnetization  $M_s$  with maximum value of 76.1 emu/g for  $x = 1.0$ . Saturation magnetization decreases when ions occupy spin-up site and increases for spin-down sites. It is observed that saturation magnetization decreases with doping

concentration till  $x = 0.6$  and then for  $x = 0.8$  and 1.0, it is quite increasing. The weak diamagnetic nature of  $\text{La}^{3+}$  can be accountable for the decrease in  $M_s$  and  $\text{Co}^{2+}$  ions have also lesser magnetic moment (3  $\mu\text{B}$ ) than  $\text{Fe}^{3+}$  ions (5  $\mu\text{B}$ ). The doping provides a nonlinear change of  $H_a$ , porosity, and grain size with all compositions. Thus, comparison among intrinsic/extrinsic points forced to nonlinear change of  $H_c$  with doping.

The ferromagnetic resonance is used with microwave absorption and can be formulated using the expression given as in Eq. 2:

$$f_r = \left(\frac{\lambda}{2\pi}\right)H_a \quad (2)$$

$f_r$  is frequency of ferromagnetic tone,  $\gamma$  is gyromagnetic proportionality, and  $H_a$  is called as anisotropy force. Also, Table 1 represents anisotropy force of distinct material compositions and resonant frequency  $f_r$  exists exterior of the examined frequency range. The microwave absorption is guided by magnetic loss of the input impedance, which is related by hysteresis parameters by the expression  $\mu'' = \frac{M_s}{2H_a\alpha}$  where  $M_s$  is saturation magnetization,  $H_a$  is anisotropy field, and  $\alpha$  is extinction coefficient. The change in  $M_s/H_a$  (Table 1) is according to the change of magnetic loss. Therefore, hysteresis parameters also contribute to microwave frequency absorption.

Table 1 provides a fast drop in  $H_a$  with  $x = 0.8$  and  $x = 1.0$ . Unsaturated state is shown by a big slope with composition  $x = 0.0$  at great value of field, which shows movement from unsaturated condition to saturated condition. The decrease in anisotropy field found from saturation law commits with this variation.

**Table 1** Lattice and hysteresis parameters of M-type  $\text{Ba}_{0.5}\text{Sr}_{0.5}\text{Co}_x\text{La}_x\text{Fe}_{12-2x}\text{O}_{19}$  hexaferrites

$x$	$a$ (Å)	$c$ (Å)	$c/a$	Cell volume (Å <sup>3</sup> )	Density		Porosity (%)	$H_c$ (Oe)	$H_a$ (kOe)	$M_s$ (emu/g)	$M_s/H_a$ (emu g <sup>-1</sup> /kOe)	$M_r$ (emu/g)	$M_r/M_s$
					XRD (g/cm <sup>3</sup> )	Bulk (g/cm <sup>3</sup> )							
0.0	5.87	23.087	3.933	689.38	5.23	3.98	23.93	325	9.67	58.1	6.00	9.2	0.164
0.2	5.876	23.091	3.929	690.91	5.34	3.88	30.02	33	7.76	68.6	8.84	3.2	0.053
0.4	5.878	23.115	3.932	692.10	5.46	4.19	19.76	900	10.45	62.1	5.94	19	0.394
0.6	5.882	23.127	3.931	693.40	5.57	4.37	24.87	48	8.34	52.4	6.28	6.0	0.096
0.8	5.885	23.135	3.931	694.35	5.68	3.62	27.87	37	6.15	70.5	11.62	5.2	0.097
1.0	5.888	23.141	3.930	695.24	5.80	4.28	33.75	36	7.56	76.1	10.06	7.1	0.126

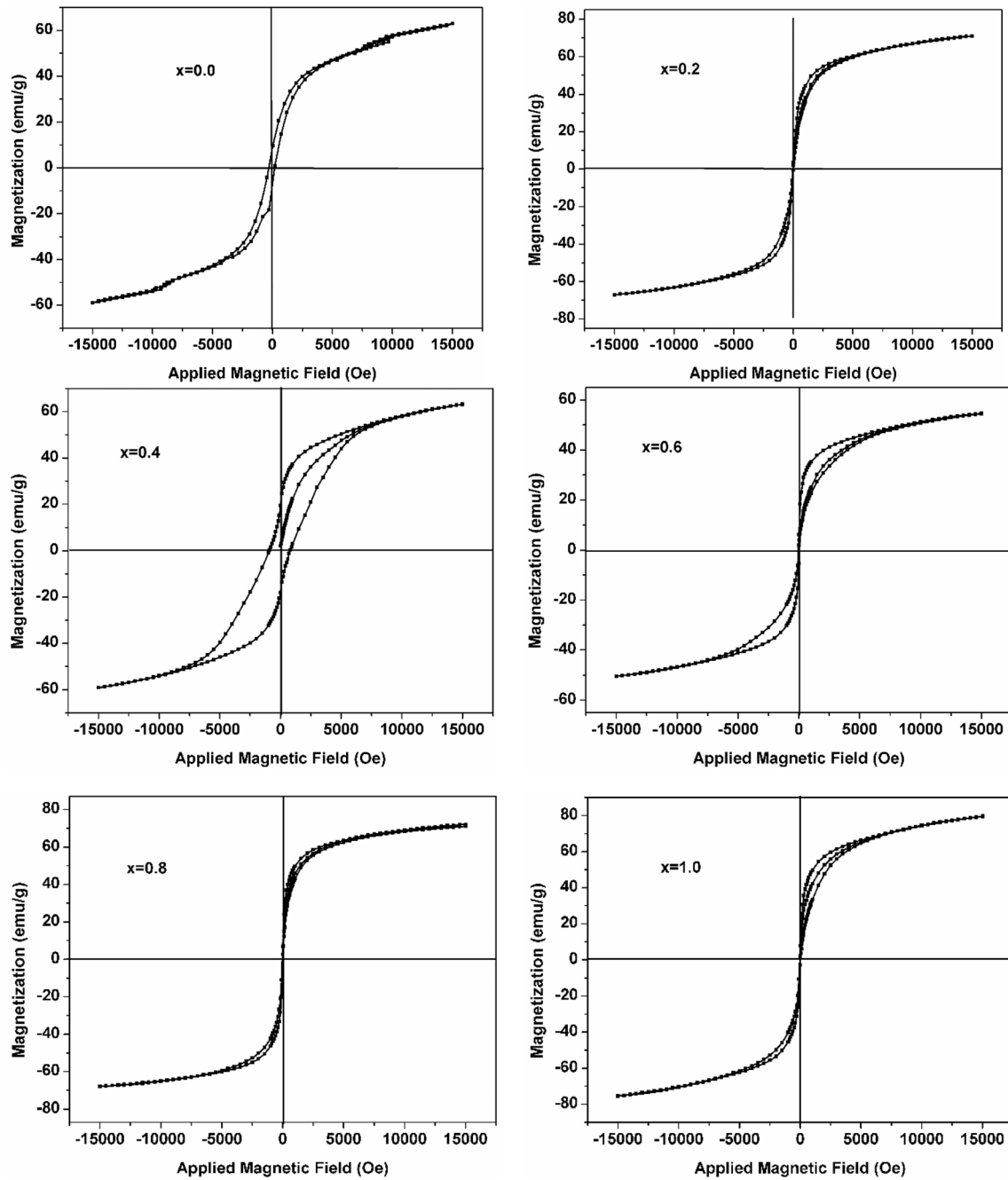


**Fig. 2** Hysteresis curves of ferrite  $Ba_{0.5}Sr_{0.5}Co_xLa_xFe_{12-2x}O_{19}$  with compositions ( $0.0 \leq x \leq 1.0$  with steps of  $x = 0.2$ )

As per Brown Equation, specific saturation of  $Ba_{0.5}Sr_{0.5}Co_xLa_xFe_{12-2x}O_{19}$  can be calculated.

$$M = M_s \left( 1 - \frac{b}{H^2} \right) \tag{3}$$

where  $M$  is the experimental specific magnetization,  $M_s$  represents the specific saturation magnetization,  $b$  is a constant which having correlation with  $H_a$ , i.e., magneto crystalline anisotropy. The specific

magnetization is plotted against the  $1/H^2$  (Fig. 3). Then trendline over the curve obtained gives the intercept as  $M_s$  and slope  $(-M_s b)$  gives the value of constant  $b$ .

Fourier transform infrared spectrum (FTIR) was analyzed using Perkin–Elmer spectrophotometer having model no. 1430. FTIR spectra with ( $0.0 \leq x \leq 1$  with steps of  $x = 0.2$ ) compositions and wavenumber region within  $(300 \text{ to } 600) \text{ cm}^{-1}$  are



represented in Fig. 4. Then, examined microwave absorption band characteristics,  $\nu_1$  near  $475\text{ cm}^{-1}$  and  $520\text{ cm}^{-1}$  and  $\nu_2$  near  $360\text{ cm}^{-1}$ , are concerned with M-type hexagonal ferrite's tetrahedral and octahedral sites: stretching vibrations of metal oxide  $\text{Fe}^{3+}\text{-O}^{2-}$  are concerned to these bands. The variation in gap between tetrahedral and octahedral organization causes the positional variation of these bands.

### 3.3 Reflection loss and microwave power absorption

The variations of reflection loss w.r.t frequency from 8.2 to 12.4 GHz at different values of thicknesses are explored in Fig. 5. Reflection loss enhances with small doping of  $\text{Co}^{2+}$  &  $\text{La}^{3+}$  and RL is more than  $-10\text{ dB}$  for most of the region in X-band. Composition  $x = 0.0, 0.2, 0.4,$  and  $0.6$  shows max RL of  $-23.61\text{ dB}, -43.73\text{ dB}, -12.58\text{ dB},$  and  $-16.01\text{ dB}$ , respectively, at different frequencies. Besides that, these are showing the same behavior for wide range of bandwidths. So, the composed material can be used as good microwave absorber for a number of wideband and narrowband applications. The thickness also plays a vital role while deciding the particular application. Because all compositions showing their best responses for different thickness values. It means that we can control the absorbing properties by controlling the frequency, composition, and thickness as well.

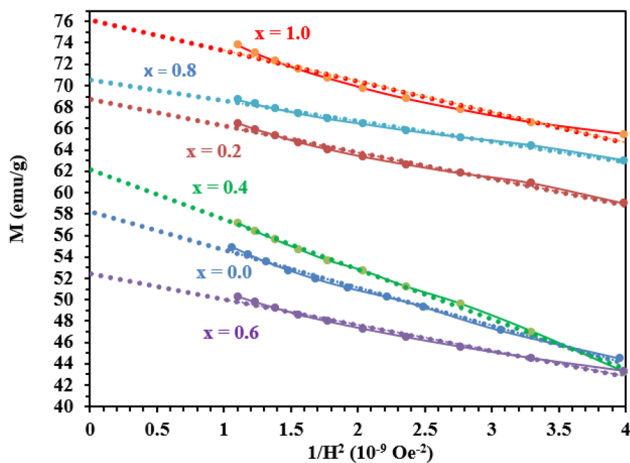


Fig. 3 Plot of  $M$  versus  $1/H^2$  for  $\text{Ba}_{0.5}\text{Sr}_{0.5}\text{Co}_x\text{La}_x\text{Fe}_{12-2x}\text{O}_{19}$

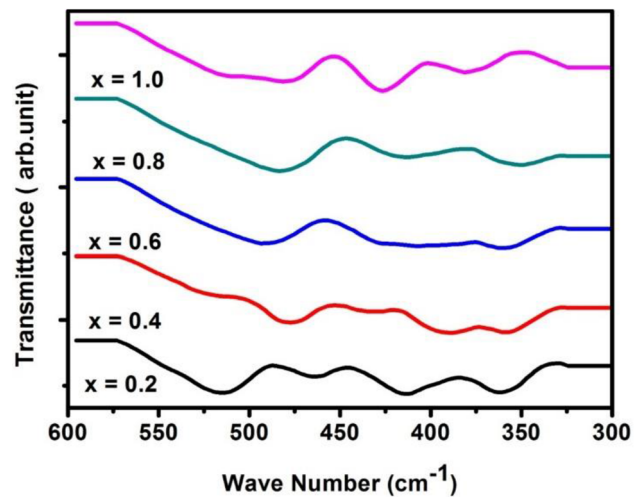


Fig. 4 Fourier transform infrared spectrum (FTIR spectra) with  $(0.0 \leq x \leq 1$  with steps of  $x = 0.2$ )

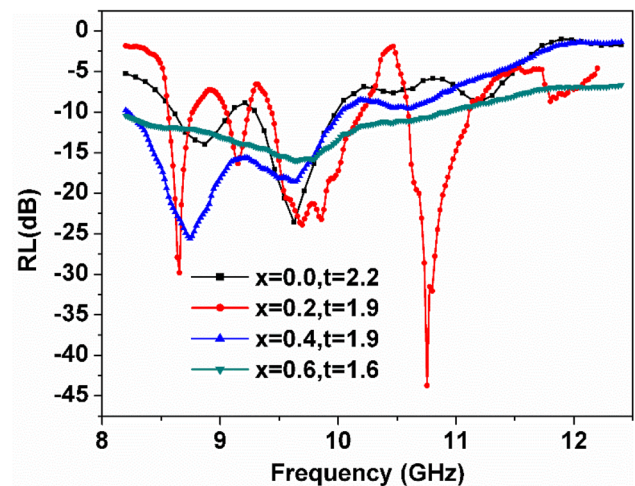


Fig. 5 Variations of RL peaks w.r.t frequency of  $\text{Ba}_{0.5}\text{Sr}_{0.5}\text{Co}_x\text{La}_x\text{Fe}_{12-2x}\text{O}_{19}$  ( $x = 0.0, 0.2, 0.4, 0.6$ )

### 3.4 Quarter wavelength ( $\lambda/4$ ) method

With this method, as ferrite thickness is equivalent to  $(\lambda/4)$  of microwave frequency signal, it will be absorbed/attenuated when passing within ferrite material. As the microwave frequency signal travels within ferrite sample and backed through metal plate, some portion of the microwave frequency signal can be reflected with the anterior surface area of ferrite material along with residual of frequency signal which travels through ferrite sample. This traveled signal will be reflected when going to the metal plate, then comes over at the ferrite's front face. As frequency signal reflected from the anterior face of

ferrite and reflected frequency signal from metal plate both are of equal magnitude and having phase difference of 180°, then these signals will be canceled by each other and show zero reflection. This state can be represented mathematically as follows:

$$t_m = \frac{n \cdot c}{4f_m \sqrt{\mu_r \epsilon_r}} \quad \text{where } n = 1, 3, 5 \quad (4)$$

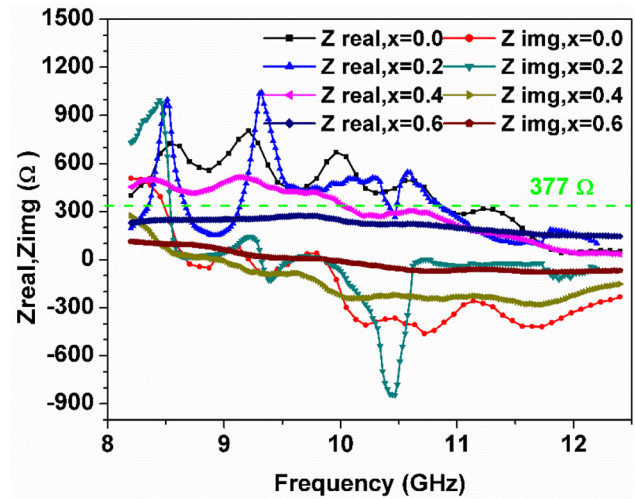
$t_m$  can be denoted as matching thickness,  $f_m$  is matching frequency,  $\mu_r$  is complex permeability, and  $\epsilon_r$  is complex permittivity, and  $c$  is velocity of light. Complex permeability and complex permittivity can be derived from S-parameters by using Nicholson–Ross technique.

Table 2 displays different parameters, which were related to quarter wavelength ( $\lambda/4$ ) mechanism for  $x = 0.0, 0.2, 0.4,$  and  $0.6$ . The mechanism of quarter wavelength is used with above-said compositions of  $x$  to find the highest absorption and peak value of RL ( $-43.73$ ) at  $10.75$  GHz for  $x = 0.2$ , which is represented in Fig. 6. For all the compositions, measured thickness and theoretical thickness are almost equal.

Table 3 depicts bandwidth associated with all compositions. Two ranges are classified, in which firstly we find the bandwidth for all compositions at different available thickness in the range of RL varying from  $-10$  to  $-20$  dB and then for the similar cases with  $RL > -20$  dB (if available). If we see the case of composition  $x = 0.2$  with thickness of  $1.9$  mm, we are acquiring maximum RL as  $-43.73$  at frequency  $10.75$  GHz and it gives B.W as  $0.07$  GHz and  $0.19$  GHz with RL in the range of  $-10$  dB to  $-20$  dB and B.W as  $0.2$  GHz with  $RL > -20$  dB and hence can be utilized in narrowband applications. Besides that, for composition  $x = 0.6$ , it is giving wideband response with B.W  $2.7$  GHz and maximum RL as  $-16.01$  dB at frequency  $9.65$  GHz with thickness of  $1.6$  mm. It can also be observed from Table 3 that we can vary the band as per requirement with varying composition and varying thickness values too.

**Table 2**  $Z_{real}, Z_{img}$  values of RL peak at various thicknesses in  $Ba_{0.5}Sr_{0.5}Co_xLa_xFe_{12-2x}O_{19}$  hexaferrites

Composition	Frequency (GHz)	thickness	Calculated	RL (dB)	$Z_{real}$ ( $\Omega$ )	$Z_{img}$ ( $\Omega$ )
$x = 0.0$	9.62	2.2	2.15	$-23.61$	429.12	7.89
$x = 0.2$	10.75	1.9	1.54	$-43.73$	381.90	0.56
$x = 0.4$	8.74	1.82	1.9	$-25.58$	415	16.31
$x = 0.6$	9.65	1.6	1.56	$-16.01$	274.20	7.08



**Fig. 6** Impedance matching mechanism with frequency,  $Z_{real}$  and  $Z_{img}$  values corresponding to the peaks in RL parameter in  $Ba_{0.5}Sr_{0.5}Co_xLa_xFe_{12-2x}O_{19}$  ( $x = 0.0, 0.2, 0.4, 0.6$ )

### 3.5 Mechanism of impedance matching

According to transmission line theory, input impedance, i.e.,  $Z_{in}$  of a mono-layer absorber will be found conceptually and can be written as follows:

$$Z_{in} = Z_0 \sqrt{\frac{\mu_r}{\epsilon_r}} \tanh \left[ j \left( \frac{2\pi ft}{c} \right) \sqrt{\mu_r \epsilon_r} \right] \quad (5)$$

where  $Z_0$  is free space characteristic impedance and is equal to  $377\Omega$  and  $\mu, \epsilon, f, t,$  and  $c$  parameters are known as complex permeability, complex permittivity, frequency, thickness, and velocity of light in free space. If  $Z_{in} = Z_0$ , compositional input impedance is the same as characteristic impedance providing in finite signal absorption by the applied composition.

High microwave absorption is correlated to the high value of reflection loss (RL). It can be calculated by given formula:

$$RL(\text{reflectionloss}) = 20 \log \left| \frac{(Z_{in} + Z_0)}{(Z_{in} - Z_0)} \right| \quad (6)$$

$Z_{in}$  is input impedance represented in complex form that is  $Z_{in} = (a + jb)$  as given in Eq. 5, where  $a$  represents the real part and  $b$  represents imaginary part.

**Table 3** Matching thickness, matching frequency, frequency band, and absorption bandwidth for RL > - 10 dB and - 20 dB in M-type Ba<sub>0.5</sub>Sr<sub>0.5</sub>Co<sub>x</sub>La<sub>x</sub>Fe<sub>12-2x</sub>O<sub>19</sub> hexaferrites

X	Max. RL (dB)	Matching thickness (mm)	Matching frequency (GHz)	Frequency band RL > - 10 dB (GHz)	- 10 dB Absorption bandwidth (GHz)	Frequency band RL > - 20 dB (GHz)	- 20 dB absorption bandwidth (GHz)
x = 0.0	- 13.52	2.0	9.54	9.46–9.79	0.33		
	- 17.82	2.1	9.54	8.70–8.95 and 9.37–9.88	0.25 and 0.51		
	- 23.6	2.2	9.62	8.62–9.04	0.42	9.54–9.62	0.08
	- 20.9	2.3	9.62	8.62–9.04	0.42	9.62–9.71	0.09
	- 16.42	2.4	9.71	8.7–9.04 and 9.46–9.88	0.34 and 0.42		
x = 0.2	- 13.11	2.5	9.71	9.54–9.79	0.25		
	- 15.24	1.0	10.75	10.64–10.95	0.31		
	- 17.05	1.1	10.75	10.64–10.99	0.35		
	- 19.23	1.2	10.79	10.62–11.02	0.4		
	- 21.07	1.3	10.79	10.62–10.70 and 10.84–11.04	0.08 and 0.2	10.73–10.82	0.09
	- 43.73	1.9	10.75	10.59–10.66 and 10.90–11.09	0.07 and 0.19	10.68–10.88	0.2
	- 40.74	2.0	10.75	10.59–10.66 and 10.90–11.09	0.07 and 0.19	10.68–10.88	0.2
x = 0.4	- 36.65	2.1	10.75	10.59–10.64 and 10.90–11.09	0.05 and 0.19	10.66–10.88	0.22
	- 25.58	1.9	8.74	8.23–8.54 and 8.94–10.02	0.31 and 1.08	8.56–8.92	0.36
x = 0.6	- 21.11	2.0	8.67	8.2–8.51 and 8.81–9.87	0.31 and 1.06	8.58–8.79	0.21
	- 15.15	1.5	9.63	8.81–11.43	2.62		
	- 16.01	1.6	9.65	8.2–10.90	2.7		
	- 14.61	1.7	9.63	8.2–10.14	1.94		
	- 15.12	1.8	8.23	8.2–9.96	1.76		

(1) Conceptually, the whole frequency signal is absorbed if  $|Z_{in}| = Z_o$  and both are equal to  $377 \Omega$ . Thus, imaginary part of  $Z_{in}$  is zero. (2) Some absorption of RL will be observed if  $Z_{real} \neq 377 \Omega$  and  $Z_{img} \neq 0$ . If  $Z_{in}$  is approximately equal to  $Z_o$ , then due to impedance matching, maximum microwave absorption can be observed and also if there is big difference between  $Z_{in}$  and  $Z_o$  or  $Z_{img}$  increases positively or negatively, then there will be a decrease in microwave absorption.

Table 2 compiles values of  $Z_{real}$ ,  $Z_{img}$ , and  $Z_{in}$  related to maximum microwave absorption or peak values of RL found with compositions. It is clear that both  $Z_{real}$  and  $Z_{img}$  are near to  $377 \Omega$  and 0 for composition  $x = 0.2$  in comparison to  $x = 0.0, 0.4$ , and  $0.6$ . Thus, deviation found in the mechanism of quarter

wavelength with  $x = 0.0, 0.4$ , and  $0.6$ . is related with higher augmentation of  $Z_{in}$  mechanism compared to  $x = 0.2$ . Correspondingly, compositions have  $Z_{real}$  which is farther from  $Z_o$  or  $Z_{img}$  is farther from zero for more frequencies, so RL is lower. For  $x = 0.2$ , the maximum value of  $Z_{real}$  is  $381.90 \Omega$  which is closer to  $Z_o = 377 \Omega$  and  $Z_{img}$  is  $0.56 \Omega$ , which is near to zero, so RL is maximum in  $x = 0.2$ .

## 4 Conclusions

In this paper, hexagonal ferrite Ba<sub>0.5</sub>Sr<sub>0.5</sub>Co<sub>x</sub>La<sub>x</sub>Fe<sub>12-2x</sub>O<sub>19</sub> has been prepared with the addition of Co<sup>2+</sup>-La<sup>3+</sup>-doping materials where  $0.0 \leq x \leq 1.0$  with steps of  $x = 0.2$ ). Best microwave absorption



with 97% absorption or EMI attenuation is achieved with  $x = 0.2$ , thickness of 1.9 mm, and matching frequency of 10.75 GHz. For the composition  $x = 0.2$ , it has maximum RL as  $-43.73$  and it offers B.W (0.07 GHz) as narrow bandwidth  $-10 \text{ dB} \leq \text{RL} \leq -20 \text{ dB}$  and B.W (0.2 GHz) with  $\text{RL} \geq -20 \text{ dB}$ . On the similar case, the composition offers wideband response for composition  $x = 0.6$ . In this case, we acquired B.W of 2.7 GHz with  $-10 \text{ dB} \leq \text{RL} \leq -20 \text{ dB}$  and having maximum RL as  $-16.01 \text{ dB}$  at frequency 9.65 GHz. The compositions  $x = 0.2$  (with M-type formation of ferrite) have greater participation for the mechanism of impedance mechanism.

## References

1. A. Sharbati, J.M.V. Khani, *J Mater Sci Mater Electron* **24**, 3629–3633 (2013)
2. S. Padhy, S. Sanyal, R.S. Meena, R. Chatterjee, A. Bose, *I.E.T. Microw, Antennas Propag.* **8**(3), 165–170 (2014)
3. H. Kaur, C. Singh, R. Kaur, T. Dhiman, S.B. Narang, *Eur. Phys. J. B.* **88**, 274 (2015)
4. A. Septiani, T. Kristiantoro, Dedi, N. Idayanti, Y. Taryana, *ICRAMET, Jakarta* 149–151 (2016).
5. C. Singh, R. Kaur, S.B. Narang, M. Puri, T. Dhiman, H. Kaur, *J. Elect. Mater.* **45**(10), 4908–4912 (2016)
6. S.S.S. Afghahi, M. Jafarian, Y. Atassi, *J. Nanopart Res.* **18**, 192 (2016)
7. E. Handoko, I. Sugihartono, M.A. Marpaung, Z. Jalil, M. Randa, C. Kurniawan, M. Alaydrus, *BCWSP, Jakarta* 1–4 (2017).
8. R. Joshi, C. Singh, D. Kaur, S.B. Narang, R. Jotania, J. Singh, *J. Mater. Sci. Mater. Electron.* **28**, 228–235 (2017)
9. S. Mortazavinik, M. Yousefi, *Russ. J. Appl. Chem.* **90**, 298–303 (2017)
10. J. Singh, C. Singh, D. Kaur, S.B. Narang, R. Jotania, R. Joshi, *J. Alloy. Compd.* **695**, 792–798 (2017)
11. J. Singh, C. Singh, R. Joshi, S.B. Narang, *ICICS, Phagwara* 227–228 (2018).
12. H. K. Bhatia, C. Singh and A. Marwaha, *ICICS, Phagwara* 224–226 (2018).
13. Z. Hou, J. Xiang, X. Zhang, L. Gong, J. Mi, X. Shen, K. Zhang, *J. Mater. Sci. Mater. Electron.* **29**, 12258–12268 (2018)
14. X.-J. Zhang, J.-Q. Zhu, P.-G. Yin, A.-P. Guo, A.-P. Huang, L. Guo, G.-S. Wang, *Adv. Funct. Mater.* **28**, 1800761 (2018)
15. N. Tran, D. Kim, H. Kim, S. Lee, T. Phan, B. Lee, *INTERMAG, Singapore* 1–1 (2018).
16. J. Li, X. Zhao, J. Liu, L. Zhang, C. Yang, *J. Alloy. Compd.* **777**, 954–962 (2019)
17. A. Septiani, H.I. Sanjaya, Dedi, *ICRAMET, Tangerang, Indonesia* 131–134 (2019).
18. Y. Yan, H. Xia, Y. Qiu, Z. Xu, Q.-Q. Ni, *Phys. Status Solidi A* **216**, 1900663 (2019)
19. T.T.C. Trudel, J. Mohammed, H.Y. Hafeez, B.H. Bhat, S.K. Godara, A.K. Srivastava, *Phys. Status Solidi A* **216**(16), 1800928 (2019)
20. R. Peymanfar, N. Khodamoradipoor, *Phys. Status Solidi A* **216**, 1900057 (2019)
21. S. Jiao, M. Wu, X. Yu, H. Zhang, *Adv. Eng. Mater.* **22**, 1901299 (2020)
22. H. Kaur, A. Marwaha, C. Singh, S.B. Narang, R. Jotania, Y. Bai, S.R. Mishra, D. Singh, A.S.B. Sombra, M. Ghimire, P. Dhruv, *J. Elect. Mater.* **49**, 1646–1653 (2020)
23. A.V. Trukhanov, K.A. Astapovich, M.A. Almessiere, V.A. Turchenko, E.L. Trukhanova, V.V. Korovushkin, A.A. Amirov, M.A. Darwish, D.V. Karpinsky, D.A. Vinnik, D.S. Klygach, M.G. Vakhitov, M.V. Zdorovets, A.L. Kozlovskiy, S.V. Trukhanov, *J. Alloys Compd.* **822**, 153575 (2020)
24. S.R.S. Afshar, S.M. Masoudpanah, M. Hasheminasari, *J. Elect. Mater.* **49**, 1742–1748 (2020)
25. P.N. Dhruv, S.S. Meena, R.C. Pullar, F.E. Carvalho, R.B. Jotania, P. Bhatt, C.L. Prajapat, J.P.B. Machado, T.V.C. Rao, C.B. Basak, *J. Alloys Compd.* **822**, 153470 (2020)
26. P. Kaur, S. Bahel, S.B. Narang, *J. Elect. Mater.* **49**, 1654–1659 (2020)
27. M. Jafarian, S.S.S. Afghahi, Y. Atassi, A. Loriani, *J. Magn. Magn. Mater.* **493**, 165680 (2020)
28. A. Garg, S. Goel, N. Kumari, A. Dubey, N.E. Prasad, S. Tyagi, *J. Elect Mater.* **49**, 2233–2241 (2020)
29. H. Kaur, A. Marwaha, C. Singh, S.B. Narang, R. Jotania, S. Jacobo, A.S.B. Sombra, S.V. Trukhanov, A.V. Trukhanov, P. Dhruv, *J. Alloys Compd.* **806**, 120–1229 (2019)

**Publisher's Note** Springer Nature remains neutral with regard to jurisdictional claims in published maps and institutional affiliations.